RESEARCH ARTICLE

ADVANCED
PHYSICS
RESEARCH
Open Access

www.advphysicsres.com

High Dielectric Constants in BaTiO$_3$ Due to Phonon Mode Softening Induced by Lattice Strains: First Principles Calculations

Hengkai Guo, Jack S. Baker, Wei Wu,* and Kwang Leong Choy*

High-dielectric-constant materials attract much attention due to their broad applications in modern electronics. Barium titanate (BTO) is an established material possessing an ultrahigh dielectric constant; however, a complete understanding of the responsible underlying physical mechanism remains elusive. Here a set of density-functional-theory calculations for the static dielectric tensors of barium titanate under strain has been performed. The dielectric constant increases to ≈7300 under strain. The analysis of the computed vibrational modes shows that transverse vibrational mode softening (the appearance of low-frequency modes) is responsible for this significant increase as driven by the relationship between lattice contribution for the static dielectric constant (k) and vibrational frequency (ω), i.e., $k \sim \frac{1}{\omega^2}$. The relevant vibrational mode indicates a large counter-displacement of Ti ions and O anions, which greatly enhances electrical dipoles to screen the electric field. The calculations not only interpreted experimental data on the high dielectric constants of BTO, where the lattice deformation due to the strains from the grain nanostructure plays an important role, but also pointed to exploring high-throughput calculations to facilitate the discovery of the advanced dielectric materials. Moreover, the calculations can prove useful for doped BTO, for which local strains fields can be achieved using defect engineering.

1. Introduction

Advanced dielectrics, in combination with the other material properties such as elastic and piezoelectric effects, can not only promote the performance of electronic device technologies but also provide more functionalities via the coupling between electronic properties and mechanical stresses.[1] High-dielectric-constant (high-k) materials have played a pivotal role in the research and development of capacitors,[1] central processing units (CPU),[1] flash memory,[2] dynamical random-access memory,[3] and light-emitting diodes.[4] For example, high-k materials have been widely used in CPUs as gate dielectrics to prevent electrical current leakage,[5] thus improving energy efficiency and processor performance. High-k materials can also be deployed to miniature electronic devices, such as downsizing the antenna material.[6]

Barium titanate (BaTiO$_3$, BTO) is a typical high-k material,[7] which possesses one of the highest dielectric constants (≈a million when doped with lanthanum[8]), in addition to low dielectric loss and well-established ferroelectric properties. BTO has been extensively investigated experimentally for many applications including its use in capacitors.[8–13] BTO has a cubic phase (*Pm3m*) at high temperatures (≳130 °C), a tetragonal phase (*P4mm*) at room temperature, an orthorhombic phase (*Amm2*) as the temperature decreases to ≈−66 °C, and a rhombohedral (*R3m*) phase at −90 °C.[14] Grain refinements,[7,9,12]

H. Guo, K. L. Choy[+]
UCL Institute for Materials Discovery
University College London
Malet Place, London WC1E 7JE, UK
E-mail: kwang.choy@duke.edu

J. S. Baker, W. Wu[+]
UCL Department of Physics and Astronomy
University College London
Gower Street, London WC1E 6BT, UK
E-mail: wei.wu@ucl.ac.uk

J. S. Baker
Agnostiq Inc.
325 Front St W, Toronto, ON M5Y 2Y1, Canada

**ADVANCED
SCIENCE NEWS**

www.advancedsciencenews.com

**ADVANCED
PHYSICS
RESEARCH**
Open Access

www.advphysicsres.com

application of strains,[10] substructure optimization,[11] doping,[8] and composite formation[15,16] have been explored to enhance the dielectric properties of BTO. Among these, doping rare-earth atoms has the most significant effect on the static dielectric constant, which can go up to a million by using rare-earth dopants, such as lanthanum.[8] By doping transition metal atoms, e.g., iron, the dielectric constant can also be enhanced up to hundreds of thousands.[17–19] External strains, which can deform the lattice structure, also play an important role in enhancing the dielectric constant without any doping.[12] The cooperative effect both from lattice vibrations and strain dynamics could be the key to interpret the ultrahigh dielectric constant in pristine BTO. Pristine BTO also has an extraordinary dielectric constant, which is up to ≈10 000 for the tetragonal phase and ≈110 000 for the hexagonal phase.[20–22] The scarcity of rare-earth elements required to achieve high dielectric constants limits the further development of high-k materials. We therefore need to find alternative material resources and novel physical mechanisms for enhancing dielectric constants.

In contrast to the extensive experimental work on BTO, the theoretical interpretation of the tremendous enhancement of the dielectric constant has rarely been articulated clearly from a microscopic picture. The dielectric constant larger than 100 000 might well be attributed to the Maxwell–Wagner polarization due to the charge accumulations in the phase-separated materials.[8] Recently an effective spin model has been proposed to interpret the high dielectric constant in transition-metal-doped BTO.[23] Yoon et. al. have also used an effective electrical circuit model to simulate the BTO dielectric constants.[24] However, a microscopic, especially atomic scale, theoretical description of the enhancement for pure BTO is still absent. In the meantime, the development of hybrid-exchange density functional theory (HDFT) over the last few decades has improved the study and discovery of novel high-k materials significantly, both in materials screening and microscopic mechanism revelation.[14] HDFT can balance the electron localization and delocalization through mixing the Hartree–Fock exchange with the conventional exchange-correlation density functionals, thus providing a reasonable result for the electronic structure and properties of insulators, such as the bandgap.[25] The previous first principles calculations for all the four phases suggested that HDFT is able to predict the electronic structure and phonon modes correctly.[26] Unfortunately, the HDFT calculations and the related theoretical interpretations for the static dielectric constants of BTO are still rare[27,28] although there are many experimental results[29–31] for single-crystal measurements. Previous theoretical studies have mainly focused on the electronic structure, piezoelectric properties, optical dielectric constants, and vibrational modes for BTO.[14,15,17,23,26,28,32] Moriwake et. al. have computed the static dielectric constant by using constrained force methods, but their computed results are much smaller (160 at maximum) than the experimental results.[28] On the other hand, the strain effects owing to the finite grain size in BTO turns out to be very important for the high dielectric constants as suggested by the experimental studies,[12] which has not yet been taken into account in the first principles calculations. In addition, the dielectric constants as a function of lattice deformations have been evaluated by first principles calculations for SrTiO$_3$, in which the optical phonon modes can decrease down to 50 cm^{-1} due to the lattice deformation.[33] The high dielectric constant has also been attributed to the orientational effect of the electrical dipoles as the orientations can have a much larger response than the displacive effect.[34–36] Therein, the authors have estimated the dielectric constant can go up by three orders of magnitude due to the dynamical and pseudo Jahn–Teller effects, which is consistent with experiment.

2. Results and Discussion

In this work, we have performed a large number of HDFT calculations for the static dielectric constants and the phonon spectra of the tetragonal BTO, taking into account the strain effects by deforming the original lattice unit cell in the calculations. Uchino et al. have studied the factors influencing the grain size of BTO, and found that the BTO grain size varies in the range of 1%.[37] Similar results can be seen in the report by Frey and Payne.[9] Therefore, the upper limit for the lattice deformation is set to 1.1% with 0.2% increments in our calculations. We have computed the static dielectric tensors as a function of the lattice deformation applied. As shown in **Figure 1**, ε_0^{XX}, ε_0^{YY}, and ε_0^{zz} (the diagonal terms for the static dielectric tensor) are plotted as a function of the lattice deformations along the x, y, and z directions when we have the lattice expansion (s_{xx}, s_{yy}, and s_{zz} > 0). For all the parameters used therein we can only find small dielectric constants, up to ≈6. Similarly, we have performed the calculations for the static dielectric tensors when shrinking the lattice, as shown in **Figure 2**. In contrast to the expansion, these calculations show completely different characteristics. ε_0^{XX} can go up to a maximum of ≈7300, at (s_{xx} = −1.1% s_{yy} = −1.1%, and s_{zz} = −0.1%), with a few other deformation parameters leading to the order of 1000, which is consistent with the experimental results for the pure BTO.[7,20,24,29] For ε_0^{YY}, we can see the similar large dielectric constant at (s_{xx} = −1.1% s_{yy} = −1.1%, and s_{zz} = −0.1%). The shrinkage of the lattice could occur during the formation of the grain in the materials, which might potentially induce high dielectric constant. This could be due to the dynamical and pseudo Jahn–Teller effects, which imply the importance of the orientations of the electrical dipoles. The physics behind this is that the external electrical field can orient the electrical dipoles, thus leading to strong orientational contribution to the dielectric constant. Later on, we can see that the lattice distortion will result in the phonon mode softening, which will trigger the enhancement of the dielectric constant. We can also find the components of the dielectric tensors along a particular spatial direction would follow the size of the lattice deformation applied in that direction. Besides this, only deformations close to 1% can cause a significant surge in the dielectric tensor, a result that has also been verified in other functionals such as PBE and PBE0 (not shown here). Our calculations also suggest that we can potentially realize such high dielectric constant without using transition-metal or rare-earth dopants.

Based on our calculations, we can have two important areas to explore. The first is that we can use the first principles computational data produced here as the training data set for supervised machine-learning, such as artificial neural networks,[38] to predict the new lattice deformations that can lead to even higher dielectric constants. The second is that we can elaborate experimentally on the fine-grain formation to manipulate or optimize
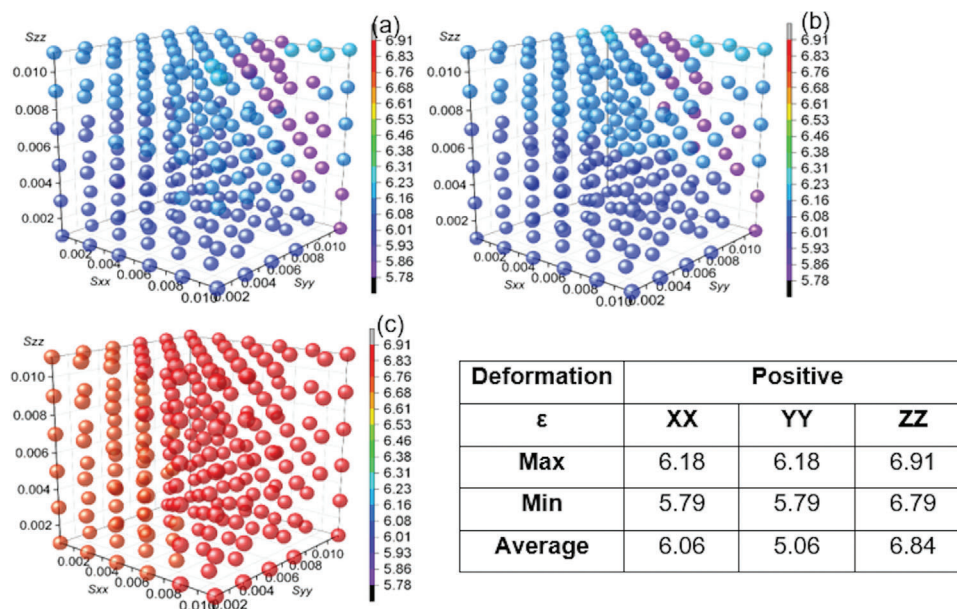
ADVANCED
SCIENCE NEWS

www.advancedsciencenews.com

ADVANCED
PHYSICS
RESEARCH
Open Access

www.advphysicsres.com

Deformation	Positive		
ε	XX	YY	ZZ
Max	6.18	6.18	6.91
Min	5.79	5.79	6.79
Average	6.06	5.06	6.84

Figure 1. The diagonal terms ε_0^{XX} a), ε_0^{YY} b), and ε_0^{ZZ} c) of the static dielectric tensor as a function of strain tensor element s_{xx}, s_{yy}, and s_{zz} (all positive, lattice expansion up to 0.011% or 1.1%). All the values can only go up to ≈ 6. In the inset table, we also show the maximum, minimum, and average values for the static dielectric tensors.
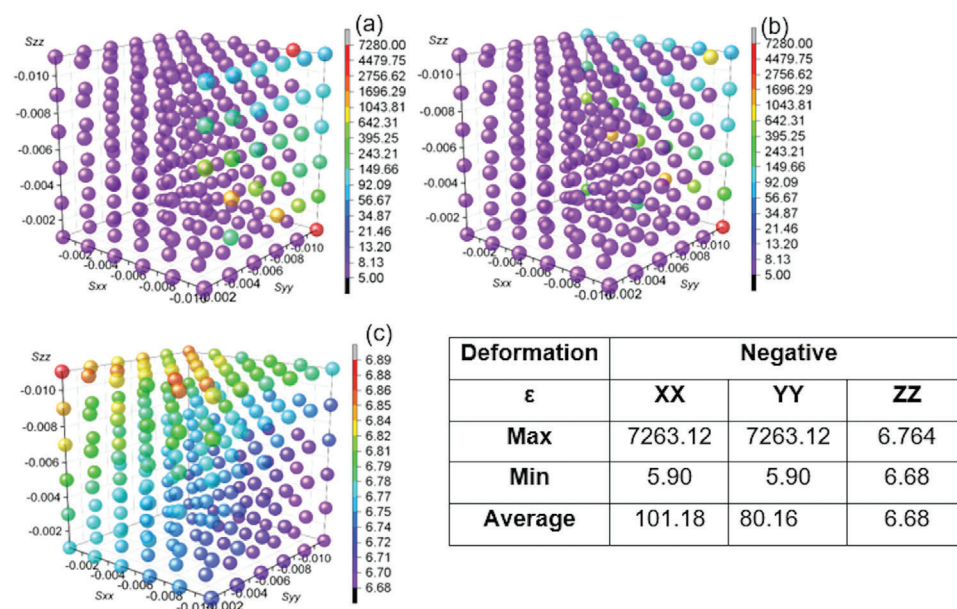

Deformation	Negative		
ε	XX	YY	ZZ
Max	7263.12	7263.12	6.764
Min	5.90	5.90	6.68
Average	101.18	80.16	6.68

Figure 2. The diagonal terms ε_0^{XX} a), ε_0^{YY} b), and ε_0^{zz} c) of the static dielectric tensor as a function of strain (all negative, lattice shrinkage down to -0.011% or -1.1%). The computed dielectric tensor diagonal terms can go up to 7263.12. In the inset table, we have also shown the maximum, minimum, and average values. We can clearly see the significant effects of the strains on the ε_0^{XX} and ε_0^{YY}.

the dielectric properties of BTO. The related experiments have shown that by decreasing the grain size below micrometres, a giant dielectric constant can be achieved in BTO.[8] The mechanism could be that the crystal is a mixture of tetragonal and so-called pseudocubic phases when the grain size decreases below some threshold value. Here the tetragonal phase will make the dominant contribution to the high dielectric constant, however, the

threshold value is yet to be studied. The relationship among the increase of the dielectric constant, the lattice deformation extent, and the threshold value for the grain size is not clear, thus requiring more investigations.

In **Figure 3**, we show the comparison between the lattice shrinkage and expansion for the calculations of the transverse optical (TO) modes and the corresponding infrared (IR) intensi-
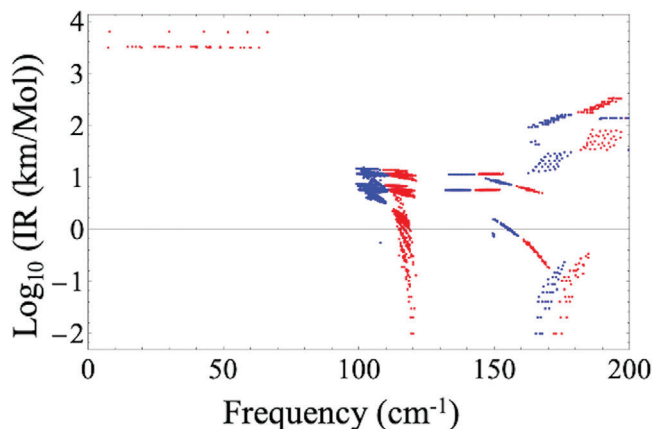
**ADVANCED
SCIENCE NEWS**

www.advancedsciencenews.com

**ADVANCED
PHYSICS
RESEARCH**
Open Access

www.advphysicsres.com

Figure 3. A comparison between the computed lowest 15 TO phonon modes for the lattice shrinkage (red) and expansion (blue) for the IR intensities as a function of phonon frequencies. We can clearly see there are many low-frequency phonon mode (softening) for the shrunk lattice. Notice that the Log_{10} (IR intensities) are plotted to show a clear contrast between different vibrational modes.

Figure 4. The contributions percentages (%) from vibrational modes with different frequencies to the dielectric constant. Here the contributions from the calculation with a large dielectric constant (≈ 7300) are in red, while the ones from a small dielectric constant (≈ 6) are in blue. We can clearly see the dominant contribution from the low frequency TO mode to the large dielectric constant, which confirms the speculation of the phonon mode softening underlying the high dielectric constant.

ties. All the calculations with large dielectric constants ($\gtrsim 1000$) have the low TO phonon mode (red on the far left), while those with small ones start from ≈ 100 cm^{-1} (in blue). This can be used to interpret the large dielectric constant for the lattice shrinkage and the small one for the lattice expansion, which is mainly due to the relationship between the static dielectric constant and the phonon frequency in Equation (1). This clearly illustrates the TO phonon mode softening due to the lattice shrinkage, while the lattice deformations cannot bring about significant changes for the longitudinal optical phonon modes, which have much higher frequencies. The lowest TO vibrational frequency (≈ 6 cm^{-1}) is mainly responsible for the high dielectric constants according to Equation (1), which shows the static dielectric constant is approximately proportional to $1/\omega^2$. Previously, the phonon softening scheme has been proposed by Homes et al. to explain the gigantic dielectric effect in similar perovskite materials $CaCu_3Ti_4O_{12}$,[39] which can be explored here to explain the high dielectric constant for BTO via lattice elastic distortions due to the grain formation and the resulting phonon mode softening. In addition, the temperature dependence of the dielectrics for $CaCu_3Ti_4O_{12}$[39] is very similar to pristine hexagonal BTO,[22] which would provide further evidence for our speculations. The appearance of the low-frequency phonon modes is due to the decrease of the ion–ion potential energies,[40] if comparing them between the high and low dielectric constants. The combination between vibrational and strain dynamics could be the source of the high dielectric constant. Here, we implicitly assume the transient dynamics induced by the lattice vibrations and strains has a smaller time scale to the lattice relaxation. Our calculations illustrate that the lattice deformations, which could result from strains during grain formation, can induce significant phonon mode softening, enhancing the dielectric constant by hundred-fold. This result is also consistent with the conclusion that the interfacial dislocation defect could be attributed to the high dielectric constant of Ni-doped BTO.[19] In addition, according to the previous research on doped BTO, our calculations could have a wide impact on the interpretation of high dielectric constant due to lattice deformation.[41–43]
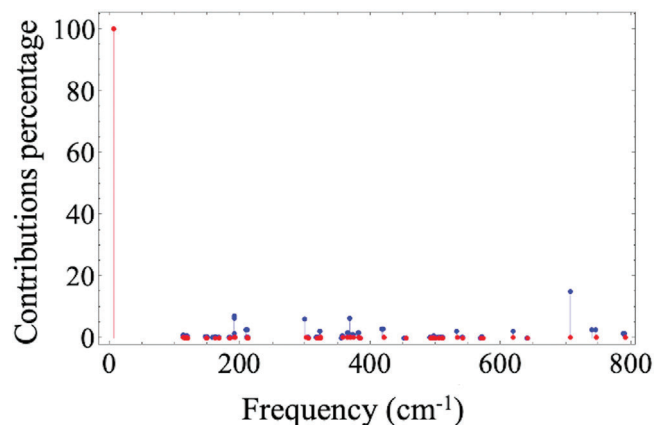
Besides, we have also found a few imaginary vibrational frequencies, which suggest that BTO has a ferroelectric instability.

As shown in Equation (1), the summation in the second term of the right-hand side, which is the lattice contribution to the static dielectric constant, consists of the contributions from different phonon modes labeled by m, i.e., $\frac{4\pi}{\Omega} \frac{Z^*_{m\alpha} Z^*_{m\beta}}{\omega_m^2}$. We can then turn this into a percentage with respect to the total static dielectric constant. In **Figure 4**, we compared the contributions from different TO vibrational modes from the calculations for a small (blue, ≈ 6) and a large (red) dielectric constant (≈ 7300). Here we plot the contributions as a function of vibrational frequencies. We can clearly see the dominance of the low-frequency TO modes (< 10 cm^{-1}) for the high dielectric constant, whereas the high-frequency modes (between 200 and 800 cm^{-1}) are populated for the small dielectric constant calculation. Moreover, we have analyzed the displacements of the atoms for the lowest-frequency mode for the calculation with the largest dielectric constant, as shown in **Figure 5**. The opposite displacements of the metallic atoms and the oxygen atoms will strengthen the electrical dipoles and are responsible for the great enhancement of the dielectric properties of BTO. Indeed, a phonon mode of this character is responsible for the cubic paraelectric to tetragonal ferroelectric phase transition in BTO, and, in our simulations, this mode is already frozen into our structure along the z-axis. Simply put, strain drives the softening of another polar mode perpendicular to the existing polar axis, which, in turn, gives rise to a dielectric anomaly.

3. Conclusions

In summary, we have performed a series of HDFT calculations for the static dielectric constants of deformed BTO based on hybrid-exchange functionals. Our calculations show that the dielectric tensors are extremely sensitive to the deformations applied to the lattice structures, which is consistent with the previous experimental results on the BTO materials with fine
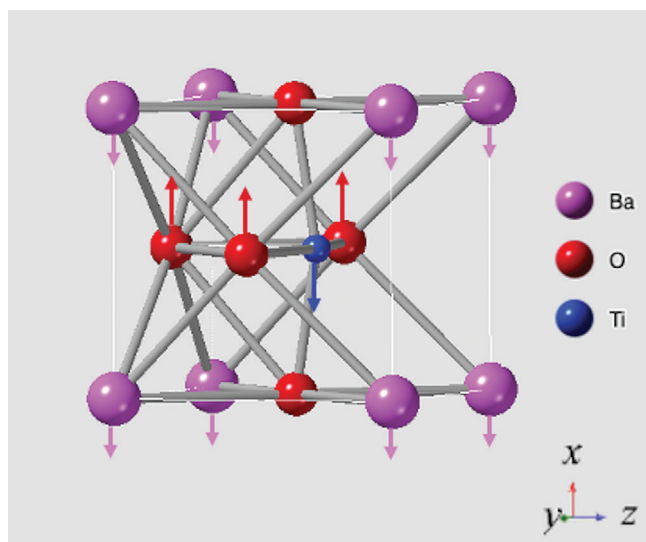
**ADVANCED
SCIENCE NEWS**

www.advancedsciencenews.com

**ADVANCED
PHYSICS
RESEARCH**
Open Access

www.advphysicsres.com

Figure 5. The displacement pattern of the ions and anions in the lowest-frequency mode for the calculation with the largest dielectric constant 7263.12 is shown. Ti and Ba (−x) move in the opposite direction as the O atoms (+x), thus enhancing the electrical dipoles and the dielectric constant.

grain structures. The highest dielectric constant is ≈7300 for the shrunk lattice structures while expanding lattice has negligible effect on the static dielectric constant. From the analysis of the computed IR intensities and phonon spectra, we can understand that the transverse optical phonon mode softening, i.e., the vibrational modes lowered by near two orders due to lattice shrinkage, is the key to trigger such high static dielectric constants. Our first-principles calculations can serve future studies of the dielectric properties of BTO (or other metal oxides). Our study can provide computational training dataset for supervised machine learning for the prediction and discovery of new material structures with even more advanced dielectric properties. The combination of high-throughput calculations and machine learning materials discovery will identify the optimal external strains, thus providing key information to improve the dielectric properties in the experiment. Our findings have not only provided the key microscopic insight to interpret a body of previous experimental results, but also pointed to a novel route to control and enhance dielectric properties by computer simulations.

4. Experimental Section

The static dielectric tensor is defined as the dielectric response of the material at low frequencies, mainly stemming from the lattice vibrations and ionic polarizations. The static dielectric constants ($\lesssim 100$ KHz) are normally dominant over the high-frequency ($\gtrsim 1$ GHz) dielectric tensor.[14,44] The HDFT calculations for the static dielectric constant of BTO using B3LYP hybrid-exchange density functional implemented in CRYSTAL14 package were performed.[25,45] The basis sets for Ba, Ti, and O have been carefully selected from the CRYSTAL code database.[46–48] The CPHF (coupled perturbed Hartree–Fock) method was used to calculate the high-frequency electron contributions to the dielectric tensor, based on density-functional perturbation theory.[49] There are three steps in the CPHF methodology, including i) the self-consistent-field (SCF) calculations, ii) the calculation of the perturbation matrices due to an electrical field, and

iii) the SC-CPHF calculations for the polarizability tensor, from which the dielectric tensors can be deduced. The CPHF methods have been employed to provide good results for many materials such as SiO_2.[50] In contrast to the finite field perturbation method, the CPHF method provides the dielectric tensor directly rather than numerically, without using zero-field extrapolations and supercells.[49] The low-frequency static dielectric tensor can be evaluated by using the eigenvalue and eigenvectors in the phonon-mode calculations[50] as follows

$$\varepsilon_0^{\alpha\beta} = \varepsilon_\infty^{\alpha\beta} + \frac{4\pi}{\Omega} \sum_m \frac{Z_{m\alpha}^* Z_{m\beta}^*}{\omega_m^2} \qquad (1)$$

Here α and β run over the x, y, and z directions. $\varepsilon_0^{\alpha\beta}$ is the static dielectric tensor, $\varepsilon_\infty^{\alpha\beta}$ is the optical dielectric tensor, Ω is the unit cell volume, ω_m is the frequency of the mth vibrational mode, and $Z_{m\alpha}^*$ is the Born effective charge for the mth vibrational mode at the α direction. Here, the elastic deformation on the lattice is also applied to model the finite grain size effect on the dielectric constant. The formalism of the strain tensor applied reads $\begin{bmatrix} s_{xx} & 0 & 0 \\ 0 & s_{yy} & 0 \\ 0 & 0 & s_{zz} \end{bmatrix}$ assuming only deforming the lattice vector individually, but not mixing them (the off-diagonal terms are zero). Here s_{xx}, s_{yy}, and s_{zz} could be larger (smaller) than 0 when expanding (shrinking) the lattice. After applying the lattice deformation (up to 1.1%) according to the experimental estimate for the internal stress,[9,12,20,37] HDFT calculations were performed to compute the phonon modes and obtain the static dielectric tensors. The self-consistent convergence tolerance for the total energy was set to 10^{-8} Hartree, and a $16 \times 16 \times 16$ Brillouin zone k-point grid was used to ensure the phonon mode calculations are sufficiently accurate.

Conflict of Interest

The authors declare no conflict of interest.

Author Contributions

K.L.C. and W.W. contributed to the conception and design of the study. H.K.G. carried out all the simulations under the supervision of W.W. and K.L.C. H.K.G., J.B., and W.W. analyzed the computational data. All the authors wrote the manuscript.

Data Availability Statement

The data that support the findings of this study are available from the corresponding author upon reasonable request.

**ADVANCED
SCIENCE NEWS**

www.advancedsciencenews.com

**ADVANCED
PHYSICS
RESEARCH**

Open Access

www.advphysicsres.com

[1] S. Krohns, P. Lunkenheimer, S. Meissner, A. Reller, B. Gleich, A. Rathgeber, T. Gaugler, H. U. Buhl, D. C. Sinclair, A. Loidl, *Nat. Mater.* **2011**, *10*, 899.

[2] C.-H. Lee, S.-H. Hur, Y.-C. Shin, J.-H. Choi, D.-G. Park, K. Kim, *Appl. Phys. Lett.* **2005**, *86*, 152908.

[3] D. E. Kotecki, J. D. Baniecki, H. Shen, R. B. Laibowitz, K. Saenger, J. J. Lian, T. Shaw, S. D. Athavale, C. Cabral Jr., P. R. Duncombe, M. Gutshe, G. Kunkel, Y. Park, Y. Y. Wang, R. Wise, *IBM J. R. Dev.* **1999**, *43*, 367.

[4] C. Soldano, *Materials* **2021**, *14*, 3756.

[5] J. Robertson, *Rep. Prog. Phys.* **2006**, *69*, 327.

[6] T. Inui, H. Koga, M. Nogi, N. Komoda, K. Suganuma, *Adv. Mater.* **2015**, *27*, 1112.

[7] W. J. Merz, *Phys. Rev.* **1949**, *76*, 1221.

[8] S. Guillemet-Fritsch, Z. Valdez-Nava, C. Tenailleau, T. Lebey, B. Durand, J.-Y. Chane-Ching, *Adv. Mater.* **2008**, *20*, 551.

[9] M. H. Frey, D. A. Payne, *Phys. Rev. B: Condens. Matter. Mater. Phys.* **1996**, *54*, 3158.

[10] T. Shi, L. Xie, L. Gu, J. Zhu, *Sci. Rep.* **2015**, *5*, 8.

[11] L. Kim, D. Jung, J. Kim, Y. S. Kim, J. Lee, *Appl. Phys. Lett.* **2003**, *82*, 2118.

[12] T. Hiramatsu, T. Tamura, N. Wada, H. Tamura, Y. Sakabe, *Mater. Sci. Eng. B* **2005**, *120*, 55.

[13] F. Chen, Y. Zhu, S. Liu, Y. Qi, H. Y. Hwang, N. C. Brandt, J. Lu, F. Quirin, H. Enquist, P. Zalden, T. Hu, J. Goodfellow, M.-J. Sher, M. C. Hoffmann, D. Zhu, H. Lemke, J. Glownia, M. Chollet, A. R. Damodaran, J. Park, Z. Cai, I. W. Jung, M. J. Highland, D. A. Walko, J. W. Freeland, P. G. Evans, A. Vailionis, J. Larsson, K. A. Nelson, A. M. Rappe, et al., *Phys. Rev. B* **2016**, *94*, 180104(R).

[14] Q.-J. Liu, N.-C. Zhang, F.-S. Liu, H.-Y. Wang, Z.-T. Liu, *Opt. Mater.* **2013**, *35*, 2629.

[15] S. Jayanthi, T. R. N. Kutty, *J. Mater. Sci.* **2005**, *16*, 269.

[16] M. Valant, A. Dakskobler, M. Ambrozic, T. Kosmac, *J. Eur. Ceram. Soc.* **2006**, *26*, 891.

[17] B. Luo, X. Wang, E. Tian, H. Song, Q. Zhao, Z. Cai, W. Feng, L. Li, *J. Eur. Ceram. Soc.* **2018**, *38*, 1562.

[18] T. A. Tuan Sulong, R. A. Maulat Osman, M. S. Idris, Z. A. Zahid Jamal, *EPJ Web Conf.* **2017**, *162*, 01050.

[19] B. C. Pecharrom, F. Mlcc, *Adv. Mater.* **2010**, *13*, 1541.

[20] G. Arlt, D. Hennings, G. De With, *J. Appl. Phys.* **1985**, *58*, 1619.

[21] J. Zhang, B. I. Lee, *J. Am. Ceram. Soc.* **2000**, *83*, 2417.

[22] J. Yu, P.-F. Paradis, T. Ishikawa, Y. Yoda, M. Itoh, F. Kano, *Chem. Mater.* **2004**, *16*, 3973.

[23] A. T. Apostolov, I. N. Apostolova, J. M. Wesselinowa, *Phys. Status Solidi Basic Res.* **2020**, *257*, 3.

[24] D.-H. Yoon, J. Zhang, B. I. Lee, *Mater. Res. Bull.* **2003**, *38*, 765.

[25] A. D. Becke, *J. Chem. Phys.* **1993**, *98*, 5648.

[26] R. A. Evarestov, A. V. Bandura, *J. Comput. Chem.* **2012**, *33*, 1123.

[27] I. Petousis, D. Mrdjenovich, E. Ballouz, M. Liu, D. Winston, W. Chen, T. Graf, T. D. Schladt, K. A. Persson, F. B. Prinz, *Sci. Data* **2017**, *4*, 160134.

[28] H. Moriwake, C. A. J. Fisher, A. Kuwabara, T. Hashimoto, *Jpn. J. Appl. Phys.* **2011**, *50*, 09NE02.

[29] S. H. Wemple, M. Didomenico, I. Camlibel, *J. Phys. Chem. Solids* **1968**, *29*, 1797.

[30] M. Zgonik, P. Bernasconi, M. Duelli, R. Schlesser, P. Günter, M. H. Garrett, D. Rytz, Y. Zhu, X. Wu, *Phys. Rev. B* **1994**, *50*, 5941.

[31] D. Berlincourt, H. Jaffe, *Phys. Rev.* **1958**, *111*, 143.

[32] I. Petousis, W. Chen, G. Hautier, T. Graf, T. D. Schladt, K. A. Persson, F. B. Prinz, *Phys. Rev. B* **2016**, *93*, 115151.

[33] L. Kim, J. Kim, D. Jung, J. Lee, *Thin Solid Films* **2005**, *475*, 97.

[34] I. B. Bersuker, *Ferroelectrics* **2018**, *536*, 1.

[35] I. B. Bersuker, *Appl. Phys. Lett.* **2015**, *107*, 202904.

[36] I. B. Bersuker, V. Polinger, *Condens. Matter* **2020**, *5*, 68.

[37] K. Uchino, E. Sadanaga, T. Hirose, *J. Am. Ceram. Soc.* **1989**, *72*, 1555.

[38] B. D. Ripley, *Pattern Recognition and Neural Networks*, Cambridge University Press, Cambridge **2007**.

[39] C. C. Homes, T. Vogt, S. M. Shapiro, S. Wakimoto, A. P. Ramirez, *Science* **2001**, *293*, 673.

[40] R. D. King-Smith, D. Vanderbilt, *Phys. Rev. B* **1994**, *49*, 5828.

[41] M. Habib, M. H. Lee, F. Akram, M.-H. Kim, W.-J. Kim, T. K. Song, *J. Alloys Compd.* **2021**, *851*, 156788.

[42] E. Patiño, A. Stashans, *Comput. Mater. Sci.* **2001**, *22*, 137.

[43] X. Cheng, M. Shen, *Solid State Commun.* **2007**, *141*, 587.

[44] K. Yim, Y. Yong, J. Lee, K. Lee, H.o-H. Nahm, J. Yoo, C. Lee, C. Seong Hwang, S. Han, *NPG Asia Mater.* **2015**, *7*, e190.

[45] R. Dovesi, R. Orlando, A. Erba, C. M. Zicovich-Wilson, B. Civalleri, S. Casassa, L. Maschio, M. Ferrabone, M. De La Pierre, P. D'arco, Y. Noël, M. Causà, M. Rérat, B. Kirtman, *Int. J. Quantum Chem.* **2014**, *114*, 1287.

[46] A. Mahmoud, A. Erba, Kh. E. El-Kelany, M. Rérat, R. Orlando, *Phys. Rev. B: Condens. Matter Mater. Phys* **2014**, *89*, 045103.

[47] S. Piskunov, E. Heifets, R. I. Eglitis, G. Borstel, *Comput. Mater. Sci.* **2004**, *29*, 165.

[48] J. Baima, A. Erba, M. Rérat, R. Orlando, R. Dovesi, *J. Phys. Chem. C* **2013**, *117*, 12864.

[49] M. Ferrero, M. Rérat, R. Orlando, R. Dovesi, *J. Chem. Phys.* **2008**, *128*, 014110.

[50] F. Pascale, C. M. Zicovich-Wilson, F. López Gejo, B. Civalleri, R. Orlando, R. Dovesi, *J. Comput. Chem.* **2003**, *25*, 888.